Monthly Notices
of the
ROYAL ASTRONOMICAL SOCIETY

MNRAS **492,** 5003–5010 (2020) doi:10.1093/mnras/staa120

Evidence of spectral evolution on the white dwarf sample from the *Gaia* mission

G. Ourique,[1] S. O. Kepler,[1] A. D. Romero,[1]★ T. S. Klippel[1] and D. Koester[2]

[1]*Instituto de Física, Universidade Federal do Rio Grande do Sul, 91501-900 Porto-Alegre, RS, Brazil*
[2]*Institut für Theoretische Physik und Astrophysik, Universität Kiel, 24098 Kiel, Germany*

Accepted 2020 January 12. Received 2020 January 11; in original form 2019 October 22

ABSTRACT

Since the *Gaia* data release 2, several works have been published describing a bifurcation in the observed white dwarf colour−magnitude diagram for $G_{\rm BP} - G_{\rm RP} > 0$. Some possible explanations in the literature include the existence of a double population with different initial mass functions or two distinct populations, one formed by hydrogen-envelope and one formed by helium-envelope white dwarfs. We propose instead spectral evolution to explain the bifurcation. From a population synthesis approach, we find that spectral evolution occurs for effective temperatures below $\simeq$11 000 K and masses mainly between 0.64 $M_\odot$ and 0.74 $M_\odot$, which correspond to around 16 per cent of all DA white dwarfs. We also find that the *Gaia* white dwarf colour–magnitude diagram indicates a star formation history that decreases abruptly for objects younger than 1.4 Gyr and a top-heavy initial mass function for the white dwarf progenitors.

Key words: parallax – white dwarfs.

1 INTRODUCTION

The *Gaia* mission (Gaia Collaboration et al. 2016) is already one of the most important surveys for the study of white dwarfs. Since its data release 2, it has provided photometry on three bands, G, $G_{\rm BP}$ and $G_{\rm RP}$, and parallax and proper motion of more than 200 000 white dwarf candidates (Gentile Fusillo et al. 2019). It is expected that by the end of the *Gaia* mission, about 400 000 white dwarfs should be discovered. In its further releases, low-resolution spectra will be available, allowing the spectral confirmation and classification of white dwarfs (Jordan 2007). All these parameters combined could lead us to uncover the properties of white dwarfs, such as effective temperature, masses, radii, atmospheric composition and ages. Because white dwarfs comprise the endpoint of more than 97 per cent of the evolution of all stars in the Milky Way, these parameters will allow the mapping of the initial mass function (IMF) and star formation history (SFH) of the solar neighbourhood (e.g. Isern 2019).

Gaia Collaboration et al. (2018) described a bifurcation in the colour–magnitude diagram for $G_{\rm BP} - G_{\rm RP} > 0$, defining a high-luminosity and a low-luminosity region. This bifurcation is not expected for a simple population of white dwarfs. They argue that the high- and low-luminosity regions coincide with theoretical cooling sequences of 0.6 $M_\odot$ and 0.8 $M_\odot$, respectively, considering pure-hydrogen-atmosphere models from the Montreal Group (Holberg & Bergeron 2006; Kowalski & Saumon 2006; Tremblay et al. 2011; Bergeron et al. 2011). They note that two separate peaks in the mass distribution are not expected since Kleinman et al. (2013) did not report any minimum between 0.6 $M_\odot$ and 0.8 $M_\odot$ in the Sloan Digital Sky Survey (SDSS) DA mass distribution, only an extended tail for masses above 0.8 $M_\odot$. Thus, they proposed that the bifurcation is better described by two distinct evolutionary sequences of 0.6 $M_\odot$, one of pure-hydrogen and one of pure-helium white dwarfs, corresponding to the high-luminosity and the low-luminosity regions, respectively.

Considering that the bifurcation can only be seen for magnitudes $G_{\rm abs} > 11.5$ and colour $G_{\rm BP} - G_{\rm RP} > 0$ and becomes barely visible for magnitudes $G_{\rm abs} > 13.5$ and colour $G_{\rm BP} - G_{\rm RP} > 0.5$, in later sections of this work we call the region with a lower density of white dwarfs inside these limits the '*Gaia* gap'.

Several works have been published trying to explain the origin of the *Gaia* gap. El-Badry, Rix & Weisz (2018) proposed that a piecewise linear initial to final mass relation (IFMR) could describe the *Gaia* gap, since the slope variations of the IFMR induce variations in the number of stars in each mass interval. Kilic et al. (2018) argue that the El-Badry et al. (2018) hypothesis could explain the *Gaia* gap, but not the difference between the binary fractions of the main-sequence (∼50 per cent, depending on the spectral type) and the white dwarf populations (26 per cent according to Holberg et al. 2016). Kilic et al. (2018) used a population synthesis approach to study a sample of 13 928 white dwarfs within 100 pc. They estimated that 36 per cent of the population is composed of helium-atmosphere white dwarfs, assuming a Salpeter IMF (Salpeter 1955).

★ E-mail: alejandra.romero@ufrgs.br

They reported that the presence of a helium-atmosphere white dwarf population by itself cannot reproduce the *Gaia* gap and concluded that the gap is a consequence of a bifurcation in the mass distribution due to a double population, one with masses around 0.6 $M_{\odot}$, and a second with masses around 0.8 $M_{\odot}$. They attributed this massive population to mergers. Alternatively, core crystallization during the white dwarf evolution was considered as a possible explanation for the *Gaia* gap. When the white dwarf core crystallizes, it releases energy, slowing down the white dwarf cooling. However, Tremblay et al. (2019) concluded that crystallization is not responsible for the existence of the *Gaia* gap, but produces a separate low-luminosity branch in the HR diagram, the so-called Q-branch.

In this work, we investigate the effects of spectral evolution from hydrogen-envelope to helium-envelope white dwarfs. Spectral evolution in general has been discussed in several works since Shipman (1972). Chen & Hansen (2011, 2012) developed evolutionary models of hydrogen-envelope white dwarfs that undergo spectral evolution and turn into helium-envelope ones. They concluded from a population synthesis approach that spectral evolution is an essential process to be included in the white dwarf cosmochronology, considering that it changes the cooling rate of the white dwarfs. However, it is not known yet how common spectral evolution is, its relation to the white dwarf mass and effective temperature, or what its consequences in the colour–magnitude diagram are for large samples, such as the *Gaia* sample. Rolland, Bergeron & Fontaine (2018) propose that spectral evolution could be driven by convective mixing, which should occur for effective temperatures lower than 13 000 K and hydrogen masses between $\log(M_{\rm H}/M_{*}) \sim 10^{-15}$ and 10^{-6}.

Ourique et al. (2019) studied the number of spectroscopic DAs and non-DAs from Kepler et al. (2016) and Munn et al. (2017) and found that the helium to hydrogen white dwarf number ratio goes from ∼0.075 for effective temperatures around 30 000 K to ∼0.36 for effective temperatures around 11 000 K and becomes nearly constant for colder temperatures. From these results they conclude that most non-DAs are the result of spectral evolution, since the very late thermal pulse, which produces helium-envelope white dwarfs, is predicted not to occur for more than 0.16–0.25 of all white dwarfs (Blöcker 2001; Lawlor & MacDonald 2006). Ourique et al. (2019) also calculated the mass distribution of spectroscopic white dwarfs classified as DA, DB and DC. They found that the DC mass distribution is centred around 0.7 $M_{\odot}$, while the DA mass distributions present a decrease in number in the same region. They concluded that this decrease in the DA mass distribution is an indicator that a fraction of DAs with masses around 0.7 $M_{\odot}$ undergo spectral evolution, turning into DCs. It is important to notice that Ourique et al. (2019) used a pure-helium model to estimate parameters for non-DAs, which should lead to an overestimation in their masses (Bergeron et al. 2019; Serenelli, Rohrmann & Fukugita 2019) if their envelopes are contaminated by hydrogen.

Bergeron et al. (2019) proposed that pure-helium-atmosphere white dwarf models do not describe non-DA white dwarfs for effective temperatures below 11 000 K. They show that pure-helium models result in higher masses than expected for non-DAs below 11 000 K, and hydrogen–helium mixed-model mass determinations agree better with the mean mass for non-DAs, similar to the conclusion by Serenelli et al. (2019). Since white dwarfs that undergo spectral evolution should present some residual hydrogen on their atmospheres, these results agree with the spectral evolution hypothesis.

So far several works have used population synthesis approaches to study properties from several white dwarf populations (e.g. Wood & Oswalt 1998; García-Berro et al. 1999; Torres et al. 2001, 2002; García-Berro et al. 2004; Chen & Hansen 2012; Torres et al. 2013; Campos et al. 2016; García-Berro & Oswalt 2016; Tremblay et al. 2016). In our work, we perform Monte Carlo population synthesis using as input the white dwarf evolutionary sequences, the SFH and the final mass function (FMF). The FMF is a function that describes the number of white dwarfs that should be formed in each mass interval. The stellar density in the colour–magnitude diagram obtained for the synthetic stars is compared to the colour–magnitude diagram from the *Gaia* white dwarf photometric candidates. The novelty of our population synthesis computation is the inclusion of spectral evolution, assuming a fast transition turning a fraction of the DAs into non-DAs. To include spectral evolution we define the spectral evolution probability, i.e. a function that describes the fraction of white dwarfs that undergo spectral evolution. We study the dependence of the spectral evolution probability on the white dwarf mass and effective temperature. Our main objective in this work is to investigate the origin of the *Gaia* gap.

This work is organized as follows. In Section 2 we describe the data sample used in this work. In Section 3 we present the simulation details and its input parameters. In Section 4 we show the results of our simulations and in Section 5 we discuss our results and present our conclusions.

2 DATA SAMPLE

In this work we use the white dwarf candidate catalogue from *Gaia* data release 2 presented in Gentile Fusillo et al. (2019). This catalogue contains 486 642 objects.

To remove low-quality objects with low probability of being white dwarfs and to limit all objects to the same magnitude limits, the following cuts are applied by us:

$$\texttt{PHOT\_G\_MEAN\_FLUX\_OVER\_ERROR} > 10 \quad (1)$$

$$\texttt{PHOT\_BP\_MEAN\_FLUX\_OVER\_ERROR} > 10 \quad (2)$$

$$\texttt{PHOT\_RP\_MEAN\_FLUX\_OVER\_ERROR} > 10 \quad (3)$$

$$\texttt{PARALLAX\_OVER\_ERROR} > 10 \quad (4)$$

$$\texttt{PHOT\_G\_MEAN\_MAG} < 20.8 \quad (5)$$

$$\texttt{PHOT\_BP\_MEAN\_MAG} < 20.8 \quad (6)$$

$$\texttt{PHOT\_RP\_MEAN\_MAG} < 20.8 \quad (7)$$

$$\texttt{TEST\_PWD} > 0.75. \quad (8)$$

TEST_PWD is the probability of a given object being a white dwarf. Gentile Fusillo et al. (2019) proposed that the high-confidence white dwarf candidates should have TEST_PWD > 0.75. Furthermore, to avoid binary white dwarfs with non-white dwarf companions, we discard objects that satisfy any of these two conditions (Kepler et al. 2019):

$$\text{If} \quad (G_{\rm BP} - G_{\rm RP}) >= 0.5: \quad G_{\rm abs} > 11.25 + 2.5 \times (G_{\rm BP} - G_{\rm RP}) \quad (9)$$

$$\text{If} \quad (G_{\rm BP} - G_{\rm RP}) < 0.5: \quad G_{\rm abs} > 10 + 5 \times (G_{\rm BP} - G_{\rm RP}). \quad (10)$$

Our final sample is composed of 91 685 white dwarf candidates.

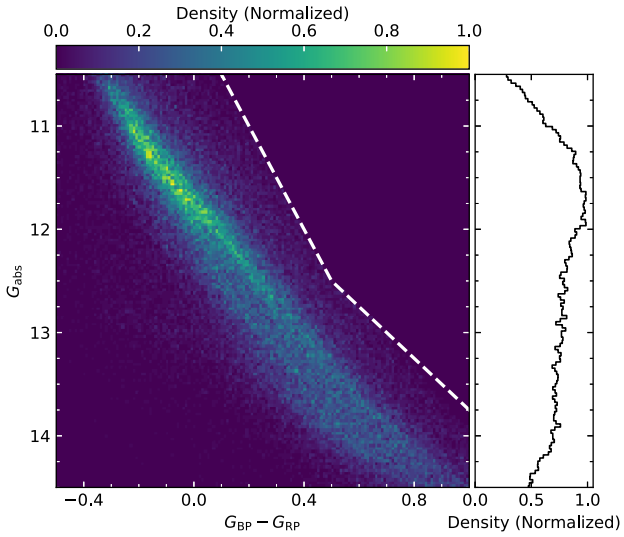

Figure 1. Hess diagram (left-hand panel) from absolute magnitude G_{abs} and colour $G_{BP} - G_{RP}$ and the luminosity function (right-hand panel) from the absolute magnitude G_{abs}. In the left-hand panel, the region limited by equations (9) and (10) is marked by a white dashed lines. The region above the white dashed line is dominated by binaries.

Due to the size of our sample, the stellar density in the colour–magnitude diagram (Hess diagram) analysis becomes a more convenient and precise tool for the analysis, as compared to the scattered stellar colour–magnitude diagram. In Fig. 1 we present the Hess diagram and the luminosity function of our sample. We have also marked in the Hess diagram the limits described by equations (9) and (10) (dashed white line).

3 SIMULATION

The main structure of our simulations is based on five components: evolutionary sequences, final mass function, star formation history, spatial distribution and spectral evolution. We describe each component below;

3.1 Evolutionary sequences

In this work we have used the hydrogen-envelope white dwarf cooling sequences with solar metallicity presented by Romero et al. (2012, 2013). From these sequences, we obtain the stellar mass, $\log(g)$, radius and effective temperature as a function of total age. We consider the evolutionary sequences with thick hydrogen envelopes, those with the largest amount of hydrogen as predicted by stellar evolution (Romero et al. 2019). The cooling sequences for non-DA white dwarfs are computed by removing the hydrogen layer from a hydrogen-atmosphere model at the pre-white dwarf phase, and evolving those models in the cooling curve.

Using a synthetic colour grid (Koester 2010; Kepler et al. 2019; Koester & Kepler 2019) we propagate our models to the colour–magnitude space, using the values of effective temperature and $\log(g)$.

3.2 Final mass function

To perform population synthesis of white dwarfs it is necessary to use a combination of the IMF (e.g. Salpeter 1955; Kroupa 2001; Chabrier 2003) and the IFMR (e.g. Ferrario et al. 2005; Kalirai et al. 2008; Romero, Campos & Kepler 2015; El-Badry et al. 2018) to describe the number of white dwarfs present in each mass interval. We define the function that describes the number of white dwarfs generated in a mass interval as the final mass function (FMF). Since it would not be possible to directly separate the effect of the IMF and the IFMR (Isern 2019), we followed a more convenient approach, that is, to define the FMF for our simulations and, from that, extract information on the IMF and the IFMR.

3.3 Star formation history

The star formation history (SFH) describes the number of white dwarf progenitors that are generated in a time interval.

The main-sequence plus giant-branch lifetime of the white dwarf progenitors is strongly dependent on the white dwarf mass. For instance, a white dwarf with a stellar mass of 0.85 $M_\odot$ and effective temperature of 30 000 K has a total age of ∼0.2 Gyr, while for a stellar mass of 0.50 $M_\odot$, the total age at the same effective temperature is ∼13.0 Gyr for the same metallicity (Romero et al. 2015).

3.4 Spatial distribution

The spatial distribution describes the density of stars that are generated according to their position relative to the Sun. Equation (11) describes the assumed spatial distribution, $\rho(r, \theta, \phi)$, where r is the distance, θ is the Galactic latitude b and ϕ is the Galactic longitude l:

$$\rho(r, \theta, \phi) = e^{-\frac{r \sin\theta}{z_v}}. \quad (11)$$

For convenience we define $z \equiv r|\sin\theta|$. The z_v parameter represents the combination of the Galactic disc height scale, z_0, and the spatial completeness of our sample.

3.5 Spectral evolution

Several processes could change the composition of the outer layers of a white dwarf during its evolution (see Fontaine & Wesemael 1987 for more details on these processes). In this work, we only consider processes that turn DAs into non-DAs during a simple evolution without external contributions. During the cooling, hydrogen-envelope white dwarfs reach effective temperatures where the hydrogen layer becomes convective. Depending on the hydrogen layer thickness, it could mix with the underlying helium layer (Koester 1976; Vauclair & Reisse 1977; Dantona & Mazzitelli 1979; Bergeron, Ruiz & Leggett 1997; Bergeron, Leggett & Ruiz 2001; Chen & Hansen 2012), turning a DA into a non-DA. This process is known as convective mixing. Castanheira & Kepler (2008, 2009), Romero et al. (2012) estimated that the distribution of the hydrogen layer mass contains a fraction between $10^{-4}\, M_H/M_*$, which is the maximum hydrogen layer mass as predicted by simple stellar evolution for a 0.6 $M_\odot$ white dwarf, and $10^{-10}\, M_H/M_*$. This wide hydrogen layer mass distribution indicates that some white dwarfs have layers thin enough to undergo spectral evolution by convective mixing at low temperatures. Diffusion is also a source of spectral evolution, but its effects are mainly important above $T_{eff} \simeq 23\,000$ K, i.e. above the observed *Gaia* gap, and therefore it will not be included in our simulation.

Rolland et al. (2018) stated that convective mixing should occur for effective temperatures below 13 000 K. Paczyński (1971), Renedo et al. (2010) and Romero et al. (2012) reported, based on an evolutionary model calculation, that massive white dwarfs present thinner hydrogen layers when compared to low-mass white dwarfs,

which makes mixing more probable (Rolland et al. 2018; Ourique et al. 2019). Finally, Tremblay & Bergeron (2008) and Tremblay et al. (2010) estimated the presence of ∼85 per cent thick hydrogen layer white dwarfs.

The existence of DBAs and DABs, i.e. white dwarfs with helium and hydrogen lines on their spectra, is evidence that mixing is not necessarily instantaneous (Bergeron et al. 1997; Chen & Hansen 2011; Rolland et al. 2018; Ourique et al. 2019). However, since we do not know the duration of these events, our approximation is that the mixing duration is much smaller than the evolutionary time-scale. In our simulations we assume that the mixing is very fast in comparison to the evolutionary time-scales, changing the evolution path of the hydrogen-envelope white dwarf into a helium-envelope white dwarf.

To include the spectral evolution in our simulations, we define a spectral evolution probability (SEP). The SEP determines the probability of a hydrogen-envelope white dwarf turning into a helium-envelope white dwarf as a function of the white dwarf mass.

3.6 Population synthesis

The synthetic population is generated by generating 1000 000 synthetic white dwarfs with hydrogen or helium envelopes with random masses, which follow the given FMF, and random ages, which follow the given SFH. A fraction of the hydrogen-envelope synthetic white dwarfs undergo spectral evolution according to their white dwarf mass and the SEP. The spectral evolution proposed in this simulation assumes that when the synthetic hydrogen-envelope white dwarf reaches a given effective temperature, it start to follows a helium-envelope cooling sequence of the same white dwarf mass. In our models, this transition is instantaneous and the only modification that is applied to the helium-envelope cooling sequence is in the white dwarf total lifetime. The lifetime of the star undergoing spectral evolution, in the helium-envelope cooling sequence at the effective temperature where the spectral evolution occurs, is defined as the same as that of the hydrogen-envelope cooling sequence at that effective temperature. The lifetime only changes from then on. For each mass, we have a model with a hydrogen envelope and other with a helium envelope in Fig. 2 (solid lines). Also, we include one representative model that starts as a hydrogen envelope and then undergoes convective mixing at 10 000 K (dashed lines). The left-hand panel represents the evolutionary path along the colour–magnitude diagram and the right-hand panel represents the effective temperature as a function of the white dwarf total age.

For each generated synthetic white dwarf, a random uncertainty is added to the magnitudes following a normal distribution similar to the uncertainty in the *Gaia* data.

3.7 Synthetic white dwarf contribution

Since brighter white dwarfs have a larger observable volume than fainter ones, it is necessary to weight each synthetic white dwarf with its observable volume. Equation (12) describes the weight associated with the observable volume and spatial distribution, $w_G(G_{\rm abs})$:

$$w_G(G_{\rm abs}) = \int_0^{2\pi}\int_{-\pi/2}^{\pi/2}\int_{d_{\rm min}}^{d_{\rm max}} \rho(r,\theta,\phi) r^2 \cos(\theta)\, {\rm d}r{\rm d}\theta{\rm d}\phi \qquad (12)$$

where $\rho(r,\theta,\phi)$ is the density described by equation (11). The radial integral limits, $d_{\rm min}$ and $d_{\rm max}$, are the minimal and maximal distances at which the object can be observed within magnitudes $G_{\rm min}$ and $G_{\rm max}$, respectively. The parameters $d_{\rm min}$ and $d_{\rm max}$ are described by equations (13) and (14), respectively:

$$d_{\rm min} = 10^{\left[1+\frac{(G_{\rm min}-G_{\rm abs})}{5}\right]} \qquad (13)$$

$$d_{\rm max} = 10^{\left[1+\frac{(G_{\rm max}-G_{\rm abs})}{5}\right]}. \qquad (14)$$

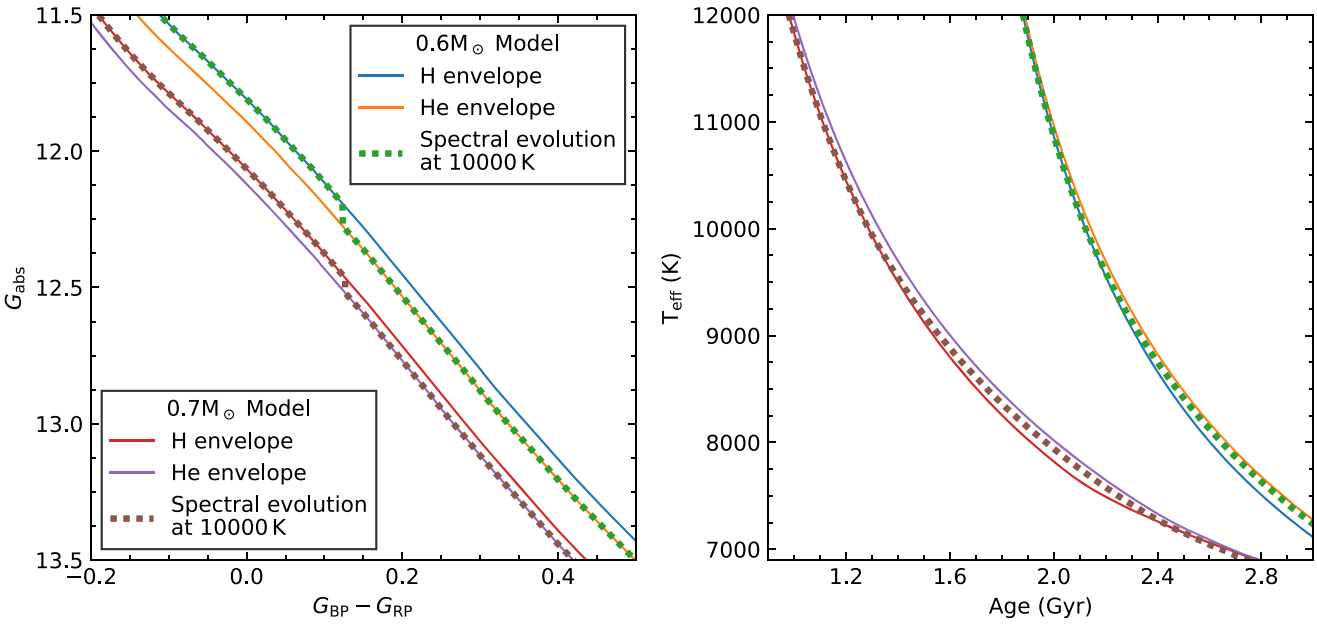

Figure 2. Evolutionary white dwarf cooling sequences. The blue and red solid lines indicate the evolutionary path for a hydrogen-envelope model with masses 0.6 $M_\odot$ and 0.7 $M_\odot$, respectively. The orange and lilac solid lines indicate the evolutionary path for a helium-envelope model with masses 0.6 $M_\odot$ and 0.7 $M_\odot$, respectively. The green and brown dashed lines indicate the path of a hydrogen-envelope model that turns into a helium-envelope model at 10 000 K due to assumed instantaneous mixing . The left-hand panel represents the evolutionary path in the colour–magnitude diagram using the absolute magnitude $G_{\rm abs}$ and the colour $G_{\rm BP} - G_{\rm RP}$. The right-hand panel indicates the evolution of the effective temperature as a function of the white dwarf total age.

The contribution of each synthetic white dwarf to the Hess diagram and the luminosity function is given by $w_G(G_{\rm abs})$.

3.8 Uncertainty

To ensure trustworthy data analysis, we resampled the magnitudes and parallaxes over the photometric and astrometric uncertainties from the *Gaia* mission data, 1000 times, assuming a normal distribution of the astrometric and photometric data, and calculated the Hess diagram and the luminosity function. For each bin in the Hess diagram and in the luminosity function, we have 1000 density determinations. From the median of these 1000 determinations we define our expected density and from the difference in the 16 per cent and 84 per cent with the median, the lower and upper density uncertainties.

Since our main focus in this work is to explain the existence of the *Gaia* gap, we limit our analysis to hydrogen-envelope white dwarf models of masses between 0.50 $M_\odot$ and 0.85 $M_\odot$, comprising the entire *Gaia* gap structure and avoiding the binary evolution region.

In the left-hand panel of Fig. 3 we show the Hess diagram of the resampled data, and in the right-hand panel, the luminosity function of the *Gaia* white dwarf candidates described in Section 2. The white dashed line on the higher luminosity diagonal of the diagram represents a hydrogen-envelope white dwarf model of 0.50 $M_\odot$, while the white dashed line on the lower luminosity diagonal represents the model of 0.85 $M_\odot$.

In Fig. 3 we can see the *Gaia* gap is centred around $G_{\rm BP} - G_{\rm RP} \simeq 0.2$ and $G_{\rm abs} \simeq 12.5$ and that there is a double peak in the luminosity function. We also notice that the density tends to zero for blue high-luminosity white dwarfs ($G_{\rm abs} < 11.5$).

To highlight the region of the *Gaia* gap, we plot in Fig. 4 – similar to Fig. 3 – the hydrogen-envelope models of 0.61 $M_\odot$ (orange line) and of 0.73 $M_\odot$ (green line), and the line of effective temperature 11 000 K (red line) and 7 000 K (cyan line).

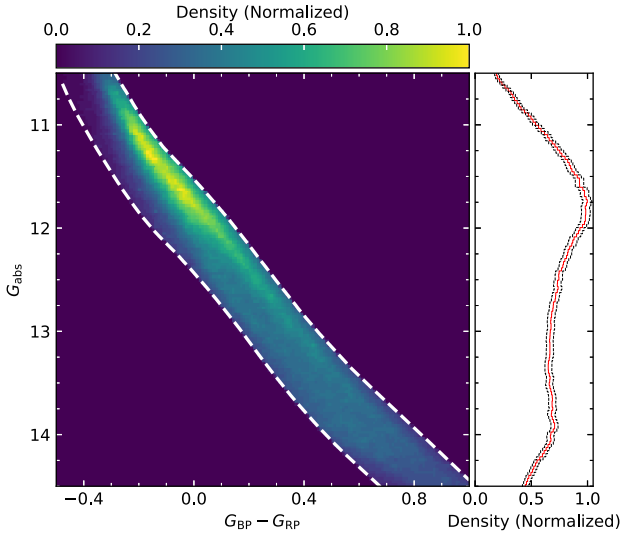

Figure 3. The Hess diagram (left-hand panel) and luminosity function (right-hand panel) of the *Gaia* white dwarf candidates resampled over their photometric and astrometric uncertainties. The width of the colour bins in the Hess diagram is 0.01 mag. The width of the magnitude bins in the Hess diagram and in the luminosity function is 0.03 mag. The white dashed lines represent our hydrogen white dwarf models of masses 0.50 $M_\odot$ (brighter) and 0.85 $M_\odot$ (fainter).

4 RESULTS

For our population synthesis input parameters, we started with a flat FMF and SFH. We varied these functions in order to minimize the quadratic difference between the Hess diagram from the *Gaia* data (Fig. 3) and the Hess diagram from the population synthesis. The same technique was used to estimate the best value for the z_v parameter, which resulted in a value around 110 pc due to our restrictions of 10σ on the parallax and photometric uncertainties.

The estimated FMF, presented in Fig. 5, shows a single peak structure around 0.55 $M_\odot$ with an extended tail for higher masses.

The SFH, presented in Fig. 6, shows an abrupt decrease in the formation rate for stars younger than 1.4 Gyr. The formation rate for ages between 1.4 Gyr and 3.5 Gyr shows a $\simeq$50 per cent increase over the mean SFH. The flat structure of the SFH for objects older than 6 Gyr is a consequence of the observed 10σ *Gaia* data not sampling these cool and faint white dwarfs.

Fig. 7 shows the Hess diagram and the luminosity function of the best synthetic model, with the FMF and SFH presented in Figs 5 and 6, respectively, with $z_v = 110$ pc and without spectral evolution. In this population synthesis, we have two populations – one of hydrogen-envelope white dwarfs, which correspond to 78 per cent of the simulated stars, and the remaining 22 per cent as helium-envelope white dwarfs. These fractions were chosen to agree with the fraction of DAs and non-DAs from the SDSS spectroscopic determinations up to data release 14 presented by Kepler et al. (2019). Our tests show that the Hess diagram and the luminosity function are very weakly sensitive to the fraction of primordial helium-envelope white dwarfs.

Fig. 8 shows the result of a very similar simulation to the one presented in Fig. 7. In this case, we changed the initial fractions of hydrogen- and helium-envelope white dwarfs to 88 and 12 per cent respectively. We included spectral evolution in this simulation with 15 per cent of DAs turning into non-DA white dwarfs at an effective temperature of 11 000 K. The non-DAs coming from spectral evolution represent 12 per cent of the total observable white

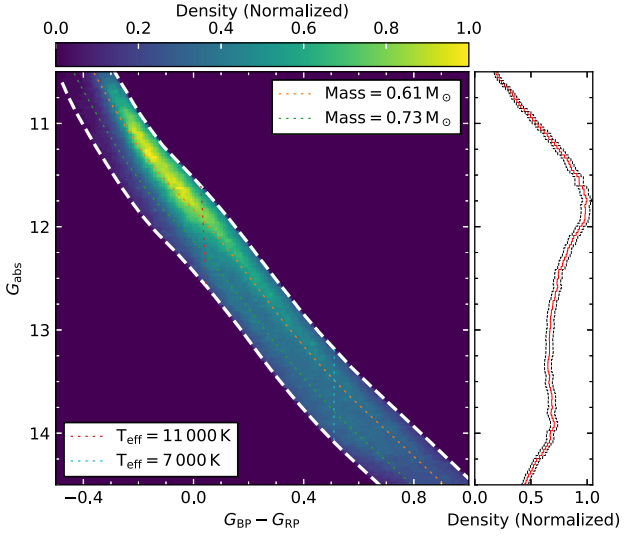

Figure 4. Same data as Fig. 3. The orange and green lines represent our hydrogen white dwarf models with 0.61 $M_\odot$ and 0.73 $M_\odot$, delimiting the *Gaia* gap in luminosity. The red and cyan lines represent the effective temperatures of 11 000 K and 7 000 K, delimiting the *Gaia* gap in colour.

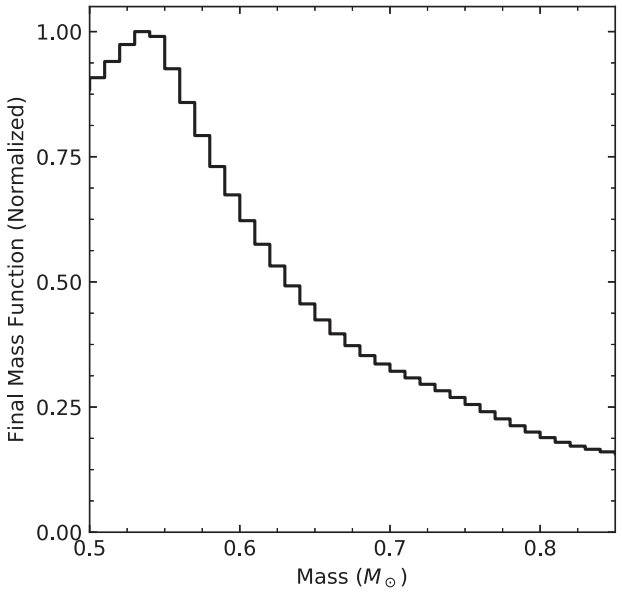

Figure 5. The estimated normalized FMF that minimizes the quadratic difference of the Hess diagram of the *Gaia* mission data and the Hess diagram of our population synthesis. The FMF presents a peak around 0.55 $M_\odot$, a very low density for masses below the peak and an extended tail for higher masses.

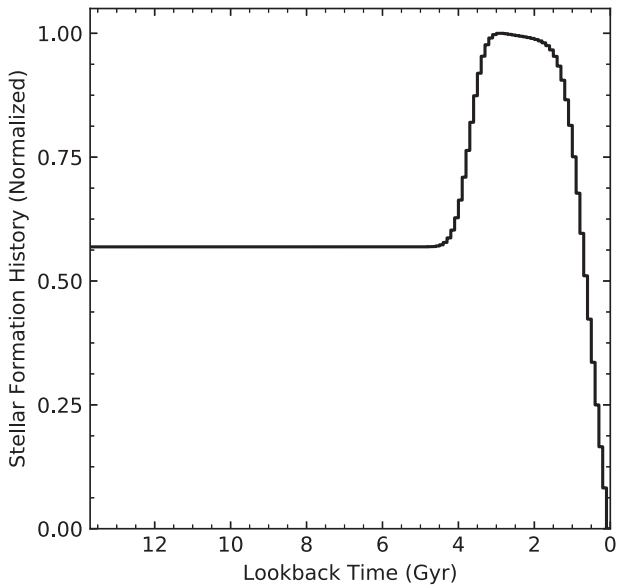

Figure 6. The estimated normalized SFH that minimizes the quadratic difference in the Hess diagram of the *Gaia* mission data and the Hess diagram of the population synthesis. The formation rate between 1.4 Gyr and 3.5 Gyr ago is $\simeq$ 50 per cent higher than the mean SFH. Also, the SFH presents a very small formation rate for very young stars and a flat formation rate for objects older than 6 Gyr.

dwarfs. These fractions were chosen to keep the final number of DAs and non-DAs similar to the values of the observed sample (Kepler et al. 2019).

The SEP used to generate the population presented in Fig. 8 defines that 68 per cent of the white dwarfs that undergo spectral evolution have masses between 0.67 $M_\odot$ and 0.74 $M_\odot$, and the spectral evolution occurs when the white dwarfs reach 11 000 K.

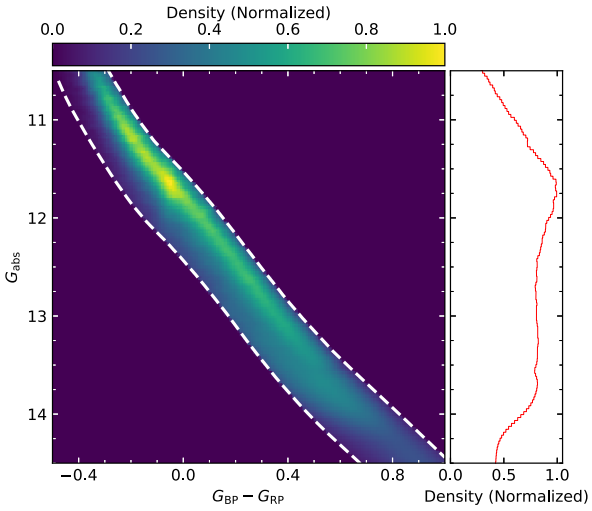

Figure 7. Hess diagram and luminosity function of the synthetic white dwarfs, generated with the FMF from Fig. 5, SFH from Fig. 6, $z_v = 110$ pc and without spectral evolution. 78 per cent of the population is composed of hydrogen-envelope white dwarfs and the remaining 22 per cent is composed of helium-envelope white dwarfs. The higher-luminosity region of the Hess diagram presents a very low density of massive objects, which is a consequence of the small recent star formation rate. The double peak in the luminosity function can be seen in the simulation. The *Gaia* gap is not reproduced in this simulation, which does not include spectral evolution. The orange and green lines represent our hydrogen white dwarf models with 0.61 $M_\odot$ and 0.73 $M_\odot$. The red and cyan lines represent the effective temperatures of 11 000 K and 7 000 K. The Hess diagram and the luminosity function are normalized to their maximum value.

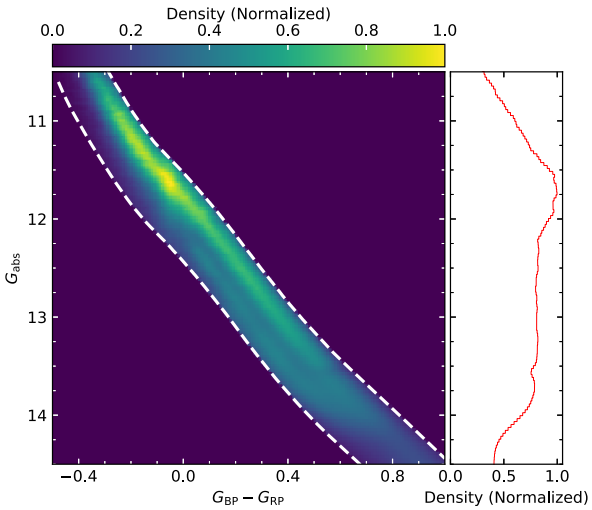

Figure 8. Hess diagram and luminosity function of the synthetic white dwarfs generated with the final mass function (FMF) shown in Fig. 5, star formation rate (SFH) shown in Fig. 6 and completeness modulated scale height $z_v = 110$ pc. 88 per cent of the population is composed of hydrogen-envelope white dwarfs and the remaining 12 per cent is composed of helium-envelope white dwarfs. In this simulation, around 15 per cent of hydrogen-envelope white dwarfs undergo spectral evolution, turning into helium-envelope white dwarfs. The features in this figure are very similar to Fig. 7, and, in this case, the *Gaia* gap is reproduced. The orange and green lines represent our hydrogen white dwarf models with 0.61 $M_\odot$ and 0.73 $M_\odot$. The red and cyan lines represent the effective temperatures of 11 000 K and 7 000 K. The Hess diagram and the luminosity function are normalized to their maximum value.

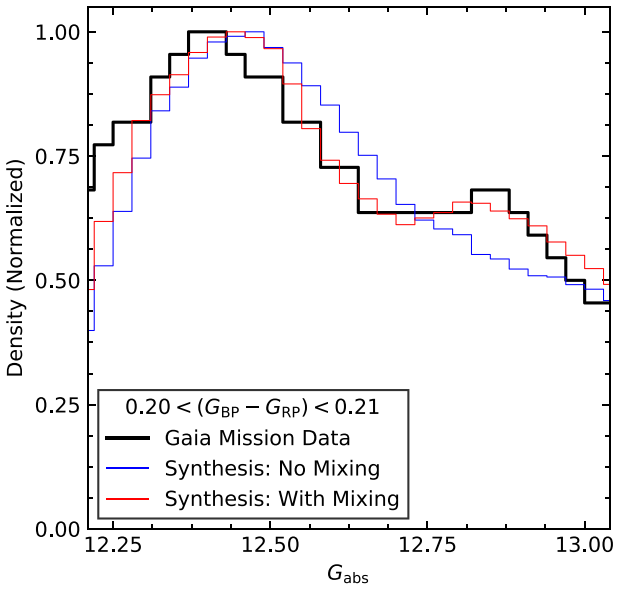

Figure 9. Density distribution of the magnitude G_{abs} for *Gaia* mission objects (black solid steps), with no spectral evolution (blue dashed steps) and for spectral evolution (red dashed steps), with colour $G_{BP} - G_{RP}$ between 0.20 and 0.21. The *Gaia* gap occurs between $G_{abs} = 12.35$ and 12.8, with a minimum around 12.7. We estimate that the *Gaia* gap corresponds to around 30 per cent of the density of white dwarfs. The density presented in this figure is normalized by the maximum density observed in the Hess diagram. The spectral evolution synthesis can reproduce the profile of the *Gaia* mission distribution, but cannot reproduce the densities accurately. Each distribution in this figure is normalized to its maximum.

In Fig. 9 we present the density distribution for the objects in our sample (black steps) and for our simulation, with (red steps) and without (blue steps) considering spectral evolution, for $G_{BP} - G_{RP}$ between 0.20 and 0.21. This figure indicates that the density of white dwarfs decreases by around 30 per cent in the *Gaia* gap in comparison to a linear decrease between the two peaks.

While our spectral evolution synthesis shows a similar profile – with the density decrease around $G_{abs} \simeq 12.75$, the synthesis without spectral evolution does not show any increase after this magnitude. As our synthesis is a simplified modelling of several existing parameters, not including, for example, the effect of metallicity and the non-instantaneous spectral evolution, we can reproduce the general features of the *Gaia* data, but we do not match accurately all regions. We have determined that the squared differences between the Hess diagram for the *Gaia* mission data and the spectral evolution synthesis are 35 per cent smaller than the synthesis with no spectral evolution.

5 DISCUSSION AND CONCLUSION

The Hess diagram for the *Gaia* mission data presented in Fig. 3 shows a gap starting around $G_{BP} - G_{RP} > 0$. The position of the centre of the *Gaia* gap corresponds to the evolutionary path of our hydrogen-envelope white dwarf sequence of mass around $0.7\,M_{\odot}$. However, since a low white dwarf formation rate with masses around $0.7\,M_{\odot}$ would be seen in the entire Hess diagram, this cannot be the explanation for the *Gaia* gap, which is only seen for $G_{BP} - G_{RP} > 0$.

We found that, in the Hess diagram of the colour–magnitude diagram, the density tends to zero for blue high-luminosity white dwarfs ($G_{abs} < 11.5$), a region that corresponds to massive young white dwarfs. In our simulation with no spectral evolution, presented in Fig. 7, we found that this behaviour is a consequence of a star formation rate that tends to zero in the last billion years (see Fig. 6), removing the presence of young massive white dwarfs in the local neighbourhood. Also, we found that the formation rate for ages between 1.4 Gyr and 3.4 Gyr is 50 per cent higher than the mean SFH.

Our best-fitting model has a completeness-corrected scale height of $z_v = 110$ pc. This value is much smaller than $z_0 = 300$ pc, estimated by Kepler et al. (2017). This is expected since the z_v parameter represents a combination of the Galactic disc scale height where the white dwarfs are immersed and the completeness of the 10σ sample from *Gaia* data release 2. The mean distance of our sample is only 190 pc.

Using the final mass function (FMF) that we obtained from our fit, we estimated the initial mass function (IMF). Using the Cummings et al. (2018) IFMR, the resulting IMF is a Salpeter-like function with a slope $\alpha = 1.07 \pm 0.02$, while using the IFMR of Romero et al. (2015) with solar metallicity we found that the slope has $\alpha = 1.38 \pm 0.01$. Both results indicate a top-heavy IMF.

Our simulations indicate that the small peak in the luminosity function for magnitudes $G_{abs}\sim14$ is a consequence of the total time that the star takes to turn into a white dwarf and reach this magnitude. For magnitudes $G_{abs}\sim13$ the age decreases towards higher masses, due to the smaller main-sequence lifetime for higher mass progenitors. However, for magnitudes $G_{abs}>13$ the age goes through an inflexion. Higher-mass white dwarfs have shorter cooling rates, leading to a longer age to reach fainter magnitudes than less-massive white dwarfs. In numbers, the ages of white dwarfs of $0.6\,M_{\odot}$, $0.7\,M_{\odot}$ and $0.8\,M_{\odot}$ at $G_{abs}\sim14$ are around 3.8 Gyr, 3.4 Gyr and 3.7 Gyr, respectively. The effect of this inflexion in the luminosity function is a pile-up of white dwarfs around $G_{abs}>13$.

Fig. 8 shows a population synthesis that includes spectral evolution in the simulation. In this case, we recovered the features from the population synthesis without spectral evolution – and the *Gaia* gap is reproduced. The SEP necessary to reproduce the *Gaia* gap implies that $\simeq$ 15 per cent of hydrogen-envelope white dwarfs undergo spectral evolution, turning into non-DAs when their effective temperature reaches $\simeq$ 11 000 K. Around 68 per cent of the white dwarfs that undergo spectral evolution have masses between $0.67\,M_{\odot}$ and $0.74\,M_{\odot}$. The fraction of white dwarfs that undergo spectral evolution corresponds to around 12 per cent of all the observable sample.

Since our simulations assume instantaneous spectral evolution, they do not reproduce accurately the density in the Hess diagram for the region that corresponds to effective temperature between 14 000 K and 11 000 K. This is an indication that spectral evolution should start around 14 000 K, partially mixing the hydrogen and helium envelopes, and reaching complete envelope transition around 11 000 K. This effective temperature range is the range where the H convection zone stars, and it is also where most DBAs are located, supporting this conclusion (Kepler et al. 2015, 2016; Eisenstein et al. 2006; Kleinman et al. 2004).

The dependence of the spectral evolution on the effective temperature is expected since it is directly related to convection episodes during the white dwarf evolution. Kepler et al. (2019) showed that the mass distribution for DBs has a mean of $0.618\pm0.004\,M_{\odot}$, assuming pure-helium atmospheres, with a very small number of DBs at higher masses, in agreement with Genest-Beaulieu & Bergeron (2019) and Ourique et al. (2019). This is an indication that the process that results in extremely thin – or non-existent –

hydrogen layer white dwarfs (probably late thermal pulse, very late thermal pulse, or merger) is not effective for the progenitors of white dwarfs with masses higher than 0.75 $M_{\odot}$.

Our simulations indicate that no more than around 16 per cent of the hydrogen-envelope white dwarfs that undergo spectral evolution have masses above 0.74 $M_{\odot}$.

Our results also indicate that more than 80 per cent of all observed helium-envelope white dwarfs, i.e. coming from spectral evolution or by primordial hydrogen deficiency, are below 12 000 K, where they do not show helium lines because of the low temperature, in agreement with the results of Ourique et al. (2019).

The significant difference in the squared difference between the Hess diagram from the *Gaia* data and the spectral evolution synthesis Hess diagram of 35 per cent, compared to that with no spectral evolution, leads us to conclude that the *Gaia* gap seen in the white dwarf distribution is a consequence of spectral evolution.

Our simulations are in agreement with the results of El-Badry et al. (2018) and Kilic et al. (2018), which show that the white dwarfs that are found at luminosities below the *Gaia* gap in the colour–magnitude diagram present a higher fraction between non-DAs and DAs.

ACKNOWLEDGEMENTS

We thank the referee for the constructive comments and suggestions that improved this manuscript. GO, ADR and SOK received support from CNPq and PRONEX-FAPERGS/CNPq (Brazil). This research has made use of theNASA Astrophysics Data System. This work has made use of data from the European Space Agency (ESA) mission *Gaia* (https://www.cosmos.esa.int/gaia), processed by the *Gaia* Data Processing and Analysis Consortium (DPAC, https://www.cosmos.esa.int/web/gaia/dpac/consortium). Funding for the DPAC has been provided by national institutions, in particular the institutions participating in the *Gaia* Multilateral Agreement.

REFERENCES

Bergeron P., Ruiz M. T., Leggett S. K., 1997, ApJS, 108, 339
Bergeron P., Leggett S. K., Ruiz M. T., 2001, ApJS, 133, 413
Bergeron P. et al., 2011, ApJ, 737, 28
Bergeron P., Dufour P., Fontaine G., Coutu S., Blouin S., Genest-Beaulieu C., Bédard A., Rolland B., 2019, ApJ, 876, 67
Blöcker T., 2001, Ap&SS, 275, 1
Campos F. et al., 2016, MNRAS, 456, 3729
Castanheira B. G., Kepler S. O., 2008, MNRAS, 385, 430
Castanheira B. G., Kepler S. O., 2009, MNRAS, 396, 1709
Chabrier G., 2003, PASP, 115, 763
Chen E. Y., Hansen B. M. S., 2011, MNRAS, 413, 2827
Chen E. Y., Hansen B. M. S., 2012, ApJ, 753, L16
Cummings J. D., Kalirai J. S., Tremblay P.-E., Ramirez-Ruiz E., Choi J., 2018, ApJ, 866, 21
Dantona F., Mazzitelli I., 1979, A&A, 74, 161
Eisenstein D. J. et al., 2006, ApJS, 167, 40
El-Badry K., Rix H.-W., Weisz D. R., 2018, ApJ, 860, L17
Ferrario L., Wickramasinghe D., Liebert J., Williams K. A., 2005, MNRAS, 361, 1131
Fontaine G., Wesemael F., 1987, in Philip A. G. D., Hayes D. S., Liebert J. W., eds, IAU Colloq. 95, Second Conference on Faint Blue Stars. p. 319
Gaia Collaboration et al., 2016, A&A, 595, A1
Gaia Collaboration et al., 2018, A&A, 616, A10
García-Berro E., Oswalt T. D., 2016, New Astron. Rev., 72, 1
García-Berro E., Torres S., Isern J., Burkert A., 1999, MNRAS, 302, 173
García-Berro E., Torres S., Isern J., Burkert A., 2004, A&A, 418, 53
Genest-Beaulieu C., Bergeron P., 2019, preprint (arXiv:1901.01857)
Gentile Fusillo N. P. et al., 2019, MNRAS, 482, 4570
Holberg J. B., Bergeron P., 2006, AJ, 132, 1221
Holberg J. B., Oswalt T. D., Sion E. M., McCook G. P., 2016, MNRAS, 462, 2295
Isern J., 2019, ApJ, 878, L11
Jordan S., 2007, in Napiwotzki R., Burleigh M. R., eds, ASP Conf. Ser. Vol. 372, 15th European Workshop on White Dwarfs. Astron. Soc. Pac., San Francisco, p. 139
Kalirai J. S., Hansen B. M. S., Kelson D. D., Reitzel D. B., Rich R. M., Richer H. B., 2008, ApJ, 676, 594
Kepler S. O. et al., 2015, MNRAS, 446, 4078
Kepler S. O. et al., 2016, MNRAS, 455, 3413
Kepler S. O., Koester D., Romero A. D., Ourique G., Pelisoli I., 2017, in Tremblay P.-E., Gaensicke B., Marsh T., eds, ASP Conf. Ser. Vol. 509, 20th European White Dwarf Workshop. Astron. Soc. Pac., San Francisco, p. 421
Kepler S. O. et al., 2019, MNRAS, 486, 2169
Kilic M., Hambly N. C., Bergeron P., Genest-Beaulieu C., Rowell N., 2018, MNRAS, 479, L113
Kleinman S. J. et al., 2004, ApJ, 607, 426
Kleinman S. J. et al., 2013, ApJS, 204, 5
Koester D., 1976, A&A, 52, 415
Koester D., 2010, Mem. Soc. Astron. Ital., 81, 921
Koester D., Kepler S. O., 2019, A&A, 628, A102
Kowalski P. M., Saumon D., 2006, ApJ, 651, L137
Kroupa P., 2001, MNRAS, 322, 231
Lawlor T. M., MacDonald J., 2006, MNRAS, 371, 263
Munn J. A. et al., 2017, AJ, 153, 10
Ourique G., Romero A. D., Kepler S. O., Koester D., Amaral L. A., 2019, MNRAS, 482, 649
Paczyński B., 1971, Acta Astron., 21, 417
Renedo I., Althaus L. G., Miller Bertolami M. M., Romero A. D., Córsico A. H., Rohrmann R. D., García-Berro E., 2010, ApJ, 717, 183
Rolland B., Bergeron P., Fontaine G., 2018, ApJ, 857, 56
Romero A. D., Córsico A. H., Althaus L. G., Kepler S. O., Castanheira B. G., Miller Bertolami M. M., 2012, MNRAS, 420, 1462
Romero A. D., Kepler S. O., Córsico A. H., Althaus L. G., Fraga L., 2013, ApJ, 779, 58
Romero A. D., Campos F., Kepler S. O., 2015, MNRAS, 450, 3708
Romero A. D., Kepler S. O., Joyce S. R. G., Lauffer G. R., Córsico A. H., 2019, MNRAS, 484, 2711
Salpeter E. E., 1955, ApJ, 121, 161
Serenelli A., Rohrmann R. D., Fukugita M., 2019, A&A, 623, A177
Shipman H. L., 1972, ApJ, 177, 723
Torres S., García-Berro E., Burkert A., Isern J., 2001, MNRAS, 328, 492
Torres S., García-Berro E., Burkert A., Isern J., 2002, MNRAS, 336, 971
Torres S., García-Berro E., Krzesiński J., Kleinman S. J., 2013, in Krzesiń;ski J., Stachowski G., Moskalik P., Bajan K., eds, Proc. Conf. held 13-17 August, 2012, at the Pedagogical University of Cracow, Poland., vol. 469, Astronomical Society of the Pacific, San Francisco, p. 109
Tremblay P.-E., Bergeron P., 2008, ApJ, 672, 1144
Tremblay P.-E., Bergeron P., Kalirai J. S., Gianninas A., 2010, ApJ, 712, 1345
Tremblay P.-E., Ludwig H.-G., Steffen M., Bergeron P., Freytag B., 2011, A&A, 531, L19
Tremblay P.-E., Cummings J., Kalirai J. S., Gänsicke B. T., Gentile-Fusillo N., Raddi R., 2016, MNRAS, 461, 2100
Tremblay P.-E. et al., 2019, Nature, 565, 202
Vauclair G., Reisse C., 1977, A&A, 61, 415
Wood M. A., Oswalt T. D., 1998, ApJ, 497, 870

This paper has been typeset from a TEX/LATEX file prepared by the author.